Article

Remote Sensing-Based Prediction of Temporal Changes in Land Surface Temperature and Land Use-Land Cover (LULC) in Urban Environments

Mohsin Ramzan [1,2] , Zulfiqar Ahmad Saqib [3,4,*] , Ejaz Hussain [1], Junaid Aziz Khan [1] , Abid Nazir [5] , Muhammad Yousif Sardar Dasti [6], Saqib Ali [7] and Nabeel Khan Niazi [3,8,*]

1   Institute of Geographical Information Systems, National University of Science & Technology (NUST), Islamabad 44000, Pakistan
2   Department of Urban & Regional Planning, University of Buffalo, Buffalo, NY 14214-8030, USA
3   Institute of Soil and Environmental Sciences, University of Agriculture Faisalabad, Faisalabad 38040, Pakistan
4   Agricultural Remote Sensing Laboratory (ARSL), National Centre of GIS and Space Application (NCGSA), Islamabad 44000, Pakistan
5   Plant and Environmental Sciences, New Mexico State University, Las Cruces, NM 88003, USA
6   School of Geoscience and Info-Physics, Central South University, Changsha 410083, China
7   Department of Computer Science, University of Agriculture Faisalabad, Faisalabad 38040, Pakistan
8   Faculty of Engineering and Science, Southern Cross University, Lismore, NSW 2480, Australia
*   Correspondence: zulfiqar.dasti@uaf.edu.pk (Z.A.S.); nabeel.niazi@uaf.edu.pk or nabeelkniazi@gmail.com (N.K.N.)

Abstract: Pakistan has the highest rate of urbanization in South Asia. The climate change effects felt all over the world have become a priority for regulation agencies and governments at global and regional scales with respect assessing and mitigating the rising temperatures in urban areas. This study investigated the temporal variability in urban microclimate in terms of land surface temperature (LST) and its correlation with land use-land cover (LULC) change in Lahore city for prediction of future impact patterns of LST and LULC. The LST variability was determined using the Landsat Thermal Infrared Sensor (TIRS) and the land surface emissivity factor. The influence of LULC, using the normalized difference vegetation index (NDVI), the normalized difference building index (NDBI), and the normalized difference bareness index (NDBaI) on the variability LST was investigated applying Landsat Satellite data from 1992 to 2020. The pixel-level multivariate linear regression analysis was employed to compute urban LST and influence of LULC classes. Results revealed that an overall increase of 41.8% in built-up areas at the expense of 24%, 17.4%, and 0.4% decreases in vegetation, bare land, and water from 1992–2020, respectively. Comparison of LST obtained from the meteorological station and satellite images showed a significant coherence. An increase of 4.3 °C in temperature of built-up areas from 1992–2020 was observed. Based on LULC and LST trends, the same were predicted for 2025 and 2030, which revealed that LST may further increase up to 1.3 °C by 2030. These changes in LULC and LST in turn have detrimental effects on local as well as global climate, emphasizing the need to address the issue especially in developing countries like Pakistan.

Keywords: land management; LST; remote sensing; climate change; surface temperature; LULC

1. Introduction

Recent climate change effects are felt all over the world and have become a priority for city authorities and scientists as ways are sought to reduce rising temperatures in urban areas and designing liveable cities. Constant modification of the structure and land use in urban areas, especially clearing of natural vegetation [1] and conversion of fertile lands into impervious surfaces, not only raises heat absorption and retaining capacity of land surface [2,3], but also indirectly leads to social and environmental degradation,

biodiversity loss and destruction of urban ecosystems throughout the globe [1,4–10]. Apart from the obvious effects, there are secondary effects on the local climate, such as alteration in wind patterns, smog, cloud development, disturbances in rate of precipitation and flash floods [11]. Thus, temperature studies of big cities are important in determining thermal comfort, energy consumption, emission of GHGs and pollutants contributing to global warming [5,12].

The phenomenon of excess heating of urban areas is widely known as the urban heat island (UHI) and can be monitored via the Land Surface Temperature (LST). The LST is a major factor in the surface energy balance by efficiently portioning latent heat and consequently the surface temperature responses as a function of varying soil moisture and vegetation cover, thus significantly affecting the local climate [8,9]. For this reason, there is an increasing trend in the recent past to study LST, or the process of UHI development and its multivariate controlling factors [11,13]. Recent spatial and temporal changes in land use-land cover (LULC) have greatly influenced LST in cities as witnessed in previous years [6,7,14].

Conventional maps alone are not sufficient to make correct decisions on land use planning or land management activities [15]. Use of satellite data is a common solution with relatively high accuracy along with vegetation indices [1,16,17]. The latest satellite products provide both, high spatial resolution e.g., Landsat and advanced space-borne thermal emission and reflection (ASTER), as well as higher temporal resolution, e.g., GOES (geostationary operational environmental satellite), AVHRR (advanced very high-resolution radiometer) and MODIS (modest resolution imaging spectroradiometer).

Moreover, use of spectral indices, such as the soil-adjusted vegetation index (SAVI), the normalized difference vegetation index (NDVI), the index of biological integrity (IBI) also called an index of biotic integrity, the modified normalized difference water index (MNDWI), the normalized difference built-up index (NDBI), the bare soil index (BSI) and the normalized difference bareness index (NDBaI) etc., along with development of computer-based models and algorithms, have made it an effective decision support tool to identify micro- or macro-climate change patterns with a minimum margin of time and error [18,19].

This study was focused on Lahore, the second largest city of Pakistan and the twenty-sixth largest city in the world. Few studies on thermal and ecological assessment are available for Lahore; most of them are based on older data, up until 2016–2017 [10,20,21]. These studies found a significant increase in urban settlements with up to a two-fold decrease in vegetation cover and concluded that future UHI increase will be the outcome of urbanization trend and resulting land use imbalances. However, there have been substantial demographic changes as well as population increase (25–30%) over the last five years. Furthermore, we are witness to extreme weather events, like heatwaves in summer and record-breaking rainfall, which warrant the need of periodic and close monitoring of such climatic changes and precise information of air temperature using LST can help to track climate change on regional and global scale using satellite remote sensing. Cities like Lahore need to evolve with the rapidly changing climate. This is the biggest urban challenge being faced by Asia and the world today, thus we need evolution of cities into 'liveable' places using precise monitoring and management to sustain economic development as well as meet global goals like UN-SDG 11 (sustainable cities and human settlements).

Therefore, the current study aims to: (1) assess the relationship of land cover changes on LST variation in the study area using different spectral indices, and (2) identify LULC and LST change patterns and then predict their impact on future scenarios using Landsat satellite data. Moreover, a comparison is made between the surface (LST) and the near-surface temperature.

2. Materials and Methods

2.1. Study Area

Lahore is Pakistan's second largest city in terms of spatial extent and population, extending from 31°15′ to 31°45′ N and 74°01′ to 74°39′ E, respectively. It is spread over an area of 405 km^2 (Figure 1) and has undulating terrain, with the highest and lowest elevations from 245 m to 142 m. Lahore has a tropical semi-arid climate (Köppen climate classification), with humid, long, and hot summers, with the monsoon season occurring from late June until August, and dry winter. The hottest month of the year is June, when temperatures routinely exceed 40 °C, and the coolest month is January with dense fog, while July is the wettest month, with heavy rain fall. The mean maximum and minimum temperatures in summer are 48 °C and 38 °C, and in winter 25 °C and −1 °C, respectively. The annual average rainfall is 628 mm (24.78 inches). The topography of Lahore is generally flat and slopes towards the south and south-west at an average gradient of 1:3000. It can be divided into two parts, i.e., the low-lying area along the River Ravi, and the comparatively upland area in the east away from Ravi (https://lahore.punjab.gov.pk/ (accessed on 16 June 2022)).
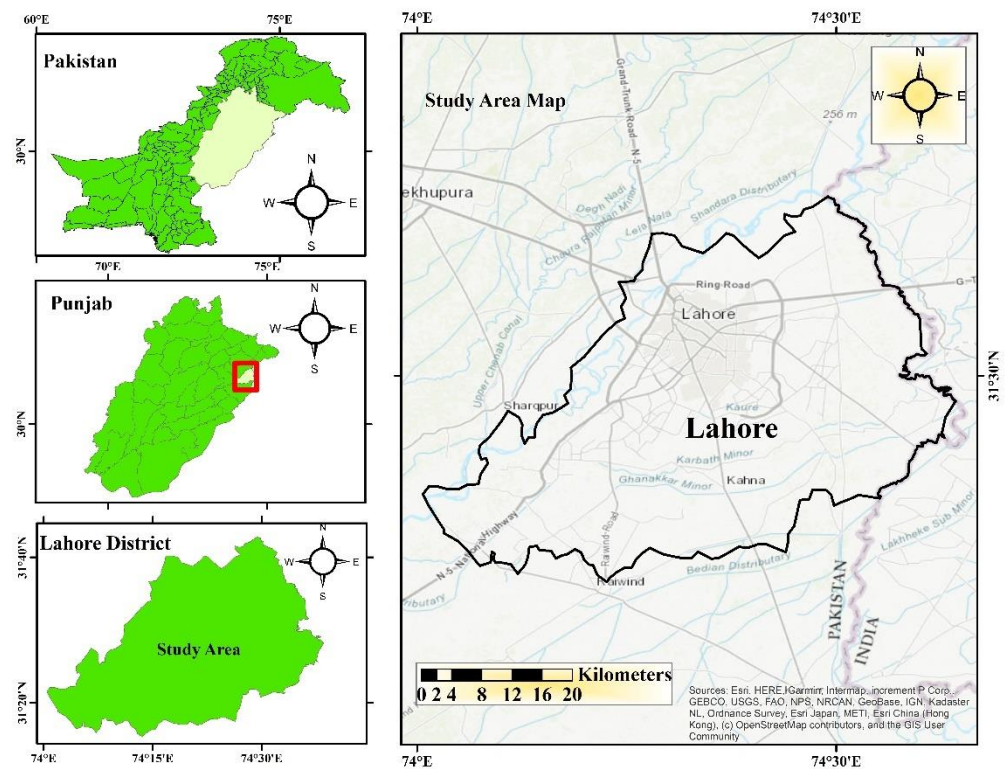

Figure 1. Study area map. Red box indicates the study area location in Punjab Province of Pakistan.

It is also the wealthiest city, with an estimated GDP of US $94 billion. It exhibits rapid environmental changes in terms of air temperature because of the high rate of urbanization. Due to recent urbanization sprawl, most of the natural land cover has been replaced by concrete and asphalt surfaces resulting in frequent urban floods and heat waves. As a result of these events, several man-made urban areas have displaced rural areas with increased thermal conductivity surfaces, resulting in higher temperatures in the urban areas as well as high LST [22,23].

2.2. Data Acquisition and Processing

The weather data, which included temperature and precipitation, was acquired from the Pakistan Meteorological Department (PMD) and collected from the Pilot Balloon Observatory weather station at Lahore (https://www.pmd.gov.pk/en/ (accessed on 18 August

2021)). As urbanization is not a very fast process and it takes years for considerable changes to take place, the images were taken within a time span of 4–6 years as described in previous studies [20,24,25]. Multispectral cloud-free satellite images of the same months from Landsat 5 TM for the years 1992, 1996, 2000 and 2008, and Landsat 8 OLI/TIRS for years 2014 and 2020, were downloaded from USGS Earth Explorer (https://earthexplorer.usgs.gov/ (accessed on 22 August 2021)). Data uniformity was maintained during downloading. After retrieving the images, they were pre-processed in ERDAS Imagine® v14 (developed by Hexagon Geospatial, Madison, AL, USA) and free open source software QGIS v3.16 (developed by Open Source Geospatial Foundation Project, Austin, TX, USA (http://qgis.osgeo.org, accessed on 22 August 2021)) for dark object subtraction (to remove haze and other anomalies), and with the bidirectional reflectance distribution function (BRDF) to remove the effects of terrain on pixels for atmospheric and radiometric corrections to ensure all had similar spectral characteristics [25]. Later, band staking was performed to unite all the bands to shape a multispectral image. Multispectral bands of both the satellites have the same spatial resolution, whereas the thermal bands (TB) were resampled using the nearest neighbour algorithm with a pixel size of 30 m to match the optical bands to avoid any conflicts for LST estimation and comparison with other results.

2.3. Methodological Formwork

The methodological formwork of the study is presented in Figure 2. Supervised classification (maximum likelihood algorithms) was applied to each image to get LULC maps for each year. Four major LULC classes, i.e., water (river, canal, lakes, and ponds, not included swamps, wetlands, and waterlogged soils), vegetation (trees, crops, forest lands, parks including urban ornamental plantation and lawns), built-up area (residential, commercial, industrial zone and scattered peri-urban settlements), and bare land were developed from each image considering their influence on LST variability. The training samples were selected with the help of Google Earth, as well as expert opinion and researcher's knowledge of the area.

Figure 2. Flow Chart of the Methodology.

To establish the relationship between LST and LULUC, 1200 random sample points (300 for each class) were taken and cross validated with Google Earth images for the

5 of 19

respective years. Statistical accuracy was also assessed using a confusion/error matrix and the kappa coefficient test. The confusion matrix provides three accuracy measures, i.e., overall accuracy, producer accuracy, and user accuracy. The overall accuracy is determined by dividing accurately classified pixels by the total number of pixels. The overall accuracy decides the classification accuracy of the entire image, whereas the producer's accuracy and the user's accuracy decide the accuracy of individual LULC classes. The producer's accuracy is calculated as the accurately classified pixels divided by the sum of total pixels in the reference image. The user's accuracy is calculated as the accurately classified pixels divided by the sum of the total pixels in the classified image. The accuracy of classification is assessed by the kappa coefficient matrix and computed as described in Equation (1) [26].

$$K = \frac{N\Sigma_{i=1}^{n} m_{ii} - \Sigma_{i=1}^{n}(G_iC_i)}{N^2 - \Sigma_{i=1}^{n}(G_iC_i)} \tag{1}$$

n = number of rows in the error matrix, i = class number, m_{ii} = number of observations in class 'i' G_i = total number of truth value in class 'i' C_i = number of predicted values in class 'i' and N = total number of classified values compared to truth values.

Parallel to image classification, different indices, such as NDVI, NDBI, and NDBaI, were applied to validate vegetation, built-up and barren areas, respectively [9,24,27,28]. Index value ranges were found to be different for different images due to variation in seasonal, atmospheric, and ground conditions of the respective images. Positive NDVI, NDBI and NDBaI values (0.2 and above) show high vegetation cover, built-up and bare land, respectively, while low or negative values show other land covers [25,27,29]. As there was a negligible change in water areas, water indices were not used. The formulas for calculating NDVI, NDBI, and NDBaI are given in Equations (2)–(4), respectively.

$$NDVI = (NIR - R)/(NIR + R) \tag{2}$$

$$NDBI = (SWIR - NIR)/(SWIR + NIR) \tag{3}$$

$$NDBaI = (SWIR - TIR)/(SWIR + TIR) \tag{4}$$

where, R = red; NIR = near infrared; SWIR = shortwave infrared; TIR = thermal Infrared.

2.4. Retrieving LST from Satellite Remote Sensing Data

The LST maps for the respective years were developed by using Equation (5). Brightness temperature (BT) used for LST was calculated following Equation (6), and land surface emissivity (LSE), as given in Equation (8), by using the Landsat satellite data provided by LPSO (2002) [30].

$$LST = \frac{BT}{1 + (\frac{W \times TB}{\sigma}) \times \ln(LSE)} \tag{5}$$

W = wavelength emitted radiance, h = Plank's constant ($6{:}626 \times 10^{-34}$ J/s)
C = light velocity ($2{:}998 \times 10^8$ m/s), σ = Boltzmann constant ($1{:}38 \times 10^{-23}$ m^2 kg s^{-2} K)

$$BT = \left(\frac{K_2}{L_n\left(\frac{K_1}{R_{TM}} + 1\right)}\right) \tag{6}$$

The K_1 and K_2 = Pre-launch calibration constants (also found in metadata MTL.txt file).
For each pixel, the digital number (DN) values of the thermal band were first converted to radiance luminance (R_{TM}) as given in Equation (7), and then converted into satellite brightness temperature (BT) using the Kelvin scale (Equation (6)).

$$R_{TM} = B_{TIR}/255\,(R_{max} - R_{min}) + R_{min} \tag{7}$$

R_{TM} = Radiance Luminance, B_{TIR} = DN values of TB i.e., (band 6 for Landsat 5 and 10 for Landsat 8), R_{max}, R_{min} = Constants (from image metadata (MTL.txt) file).

The LSE, also called surface emissivity (ε_o), was calculated by using Equation (8). This method uses NDVI values as the means for calculating the LSE from satellite image [31].

$$\text{LSE } (\varepsilon_o) = 1.009 + 0.047 \cdot \text{Ln (NDVI)} \tag{8}$$

These LST and LULC classified maps were further explored and analysed by correlating them with air temperature data from weather stations for validation of results. Because the nature of the underlying land cover can affect LST [3,22], the relationship of these factors needed to be examined. The relationship between the LULC and the resulting LST was statistically analysed by associating each LULC class with LST. After analysing the relationship between LULC change and the temperature and validating this relationship with meteorological data, the next step was to predict/forecast the future patterns and trend of LULC changes and the associated temperature using simple linear regression techniques. The trend and rate of change of LULC and LST obtained from satellite image (except 2020) were used in the regression equation to forecast for the years 2025 and 2030. The mean LST was obtained by averaging the value for all the pixels in the respective LULC class in specific Landsat based LST Images. Each value was the spatial mean of all the pixels belonging to the specific class in the image for the specific year. The estimated change was validated by comparing the predicted changes in the area for each land cover and its temperature for the year 2020 with the image derived results. After validation of the 2020 results, the values were predicted for the year 2025 and 2030, respectively.

3. Results

3.1. LULC Classification and Spectral Indices

The LULC classes were developed from satellite data and mapped as shown in Figure 3. Accuracy assessment for each classified image was also performed using the error matrix (Table 1). For the satellite images of year 1992, 1996, 2000, 2008, 2014, and 2020, the average overall classification accuracy was over 90% and with an overall kappa statistic of 0.88. The LULC classification results (which were used for prediction) for all the years were validated with ground control points taken from high resolution google earth imagery for each respective year. Accuracy assessments along with confusion matrices were also generated for each year (see Supplementary Materials for details).
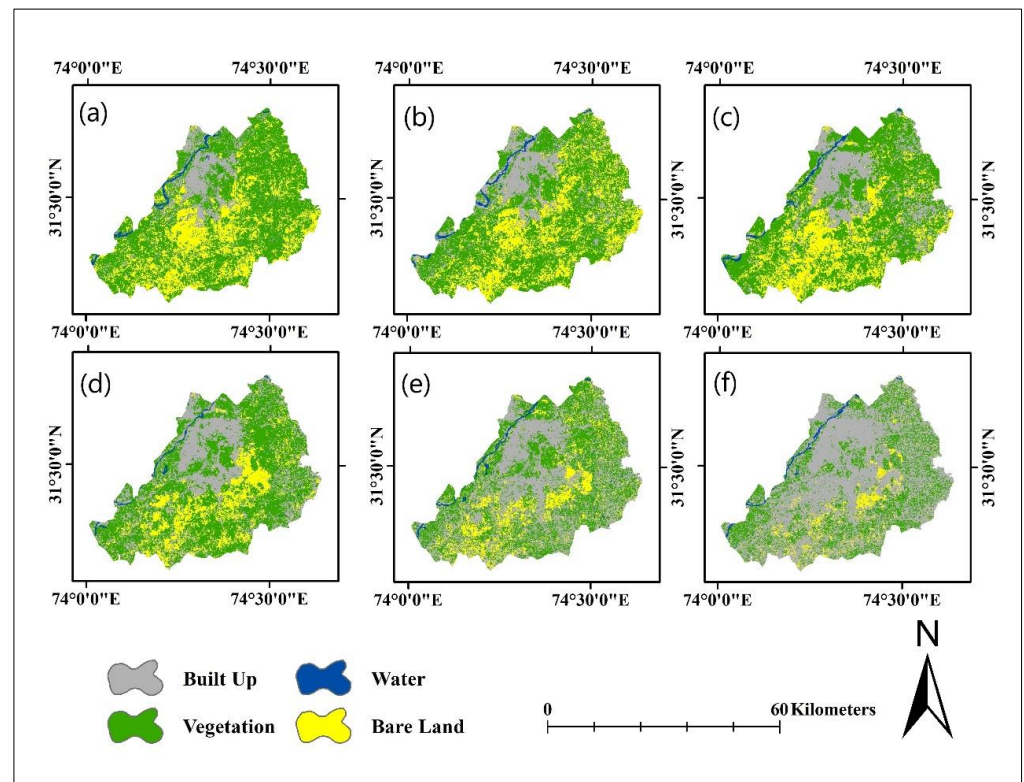
Figure 3. LULC Maps for (**a**) 1992, (**b**) 1996, (**c**) 2000, (**d**) 2008, (**e**) 2014, and (**f**) 2020, showing the spatial distribution and change in different LULC.

Table 1. Classification accuracy assessment from 1992–2017.

Dates (d/m/y)	Vegetation Cover (km²)	Built-Up (km²)	Bare Land (km²)	Water (km²)	User Accuracy (Built Up %)	Producer Accuracy (Built Up %)	Overall Kappa Statistics	Overall Accuracy
9 June 1992	1010	260.5	471.4	26.6	88.9	91.6	0.87	90.8
4 June 1996	928.5	363.26	453.6	24.8	88.2	92.3	0.89	91.2
30 May 2000	903.7	428.8	414.6	21.3	88.6	91	0.83	90.7
5 June 2008	894.9	581.2	278.2	28.4	91.7	92.3	0.9	90.3
6 June 2014	689.3	838.2	214.4	28.4	91.7	92.3	0.9	92.6
7 June 2020	590.07	1001.2	161.3	19.5	85.5	90.3	0.88	90.3

The LULC classification results for different temporal images showed that expansion of built-up land has led to a decrease in other land uses, vegetation cover being the most affected. The LULC classification analysis showed that the vegetation cover experienced a significant decrease from 1992–2020 (Figure 3). Vegetation cover area decreased from ≈1010 km² in 1992 to ≈590 km² in 2020. Similarly, areas of barren land decreased from ≈471 km² in 1992 to ≈161 km² in 2020. Built-up land showed a significant increase from ≈260 km² (which is about 14% of the Lahore's total area) in 1992 to ≈1001 km² (almost 56% of the total area) in 2020. Statistical analysis shows that about 65% of total vegetation area and 10% of the total bare land area in 1992 had changed into built-up land by 2020. Moreover, the LULC maps show that from 1992 to 2000, green areas within the core urban area have been changed into built-up area, but since then there has been very little change (Figure 4). However, after year 2000, the expansion in the built-up area is more on the out-skirts of the city, thus consuming prime agricultural land. The land cover class of water experienced a negligible change in areas throughout the study period.
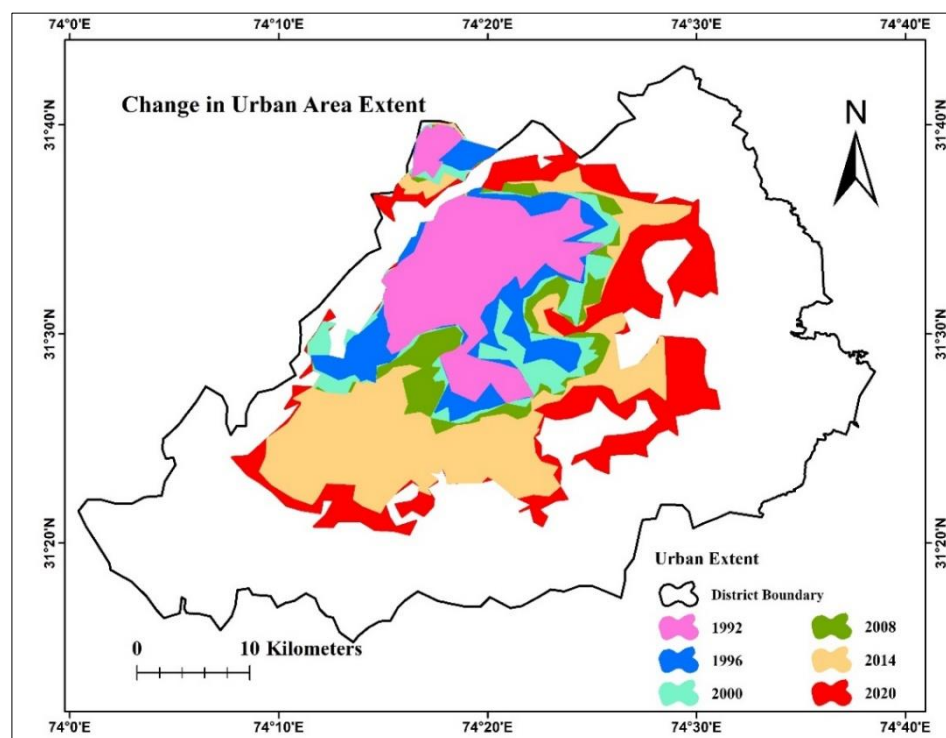
Figure 4. Change in urban built-up area and its expansion from 1992–2000 and from 2008–2020.

The error matrices revealed that there was spectral confusion between the areas of bare land and built-up land, as the two have a quite similar spectral response causing between class misclassifications [25,32].

From 1992 to 2020, Lahore has experienced drastic changes in the spatiotemporal LULC patterns. Major developments took place in the city centre where haphazard settlements gave rise to a more contiguous built-up area. Figure 4 shows the trend of temporal LULC type changes in Lahore for the study period, i.e., 1992–2020, while percentagewise LULC change analysis (Table 2), showed that built-up area has been the most rapidly growing land cover type (14.7% to 56.5%). The percentage increase in built-up area resulted in overall reduction in bare land (from 26.6% in 1992 to 9.1% in 2020), and vegetation cover (from 57% in 1992 to 33.3% in 2017, with a major decrease occurring during the period from 2008–2017) (Table 2). A look at the total percentage difference between the LULC types from 1992 to 2020 clearly shows an increase of about 41% in built-up land by 2020, at the cost of a decrease of about 23% and 17% in vegetation and bare land, respectively.

Table 2. Temporal LULC changes (in percent) for each measured year from the previous one from period 1992 to 2020 with overall change.

LULC Types	Land Cover (km^2)	Temporal LULC Change (in Percent)						Overall Change (1992–2020)
		1992	1996	2000	2008	2014	2020	
Water	26.6	1.5	1.4 (−0.1)	1.2 (−0.2)	0.9 (-1.5)	1.6 (0.7)	1.1 (−0.5)	19.5 km^2 (1.1%)
Built-Up	260.5	14.7	20.5 (5.8)	24.2 (3.7)	32.8 (8.6)	47.3 (14.5)	56.5 (9.2)	1001 km^2 (56.5%)
Vegetation	1010	57	52.4 (−4.6)	51 (−6.0)	50.5 (−0.5)	38.9 (−11.6)	33.3 (−5.6)	590 km^2 (33.3%)
Bare land	471.4	26.6	25.6 (−1.0)	23.4 (−2.2)	15.7 (−7.7)	12.1 (−3.6)	9.1 (−3.0)	161.3 km^2 (9.1%)

Values in () represent change with respect to previous monitoring year.

3.2. Spectral Indices

The NDVI, NDBI, and NDBaI values for all images developed from the Landsat 5 and Landsat 8 images for the period from 1992 to 2020 (Figures 5 and 6) collectively fell in the ranges of −0.63 to 0.71, −0.59 to 0.78, and −0.6 to 0.8, respectively. The temporal NDVI maps showed a decreasing vegetation trend in agreement with the LULC classification

result. Whereas the NDBI maps showed a slightly higher increase in built-up area in comparison to the LULC classification results. The reason for this slight difference in built-up area is because of the similar spectral response of bare land and built-up area; the NDBI index could not precisely differentiate between these two, however, the NDBaI index did. The NDBaI values showed most bare land was in June 1992 and the least bare land in June 2020. A comparison of NDBI and NDBaI indices confirmed that, bare land was decreasing at the cost of increases in built-up areas, in conformity with the LULC classification results. The purpose of using these indices was to analyse and compare the LULCs classified from the Landsat's imagery, to develop a better understanding of the relationship between NDVI, NDBI, and NDBaI indices, and LST by associating the major LULC types. Appropriate threshold values of all the indices were ascertained to help distinguish the LULC class.

3.3. Land Surface Temperature (LST)

The spatiotemporal distribution of LST over different LULC types shows a high LST in June 2020, with temperatures soaring up to approximately 46 °C (Figure 7), with a temperature of about 35.3 °C at the point of the weather station and validated with the actual temperature of that day (Table 3). An overall increasing trend in temperature in agreement with the LULC classification can be observed in the study area from 1992 to 2020, except for the year 2008, where lower temperatures (23 to 31.45 °C) were observed for different LULCs. This decrease in temperature was due to precipitation of about 12 mm on the image acquisition day (confirmed from PMD data). The June 2020 image showed the highest temperature for all LULCs compared to previous years. These results show that the higher LST, which act as proxy indicator of air temperature, seems to be influenced by multiple urban LULCs as well as other factors, such as moisture content, density of vegetation, and area of vegetation cover, etc.
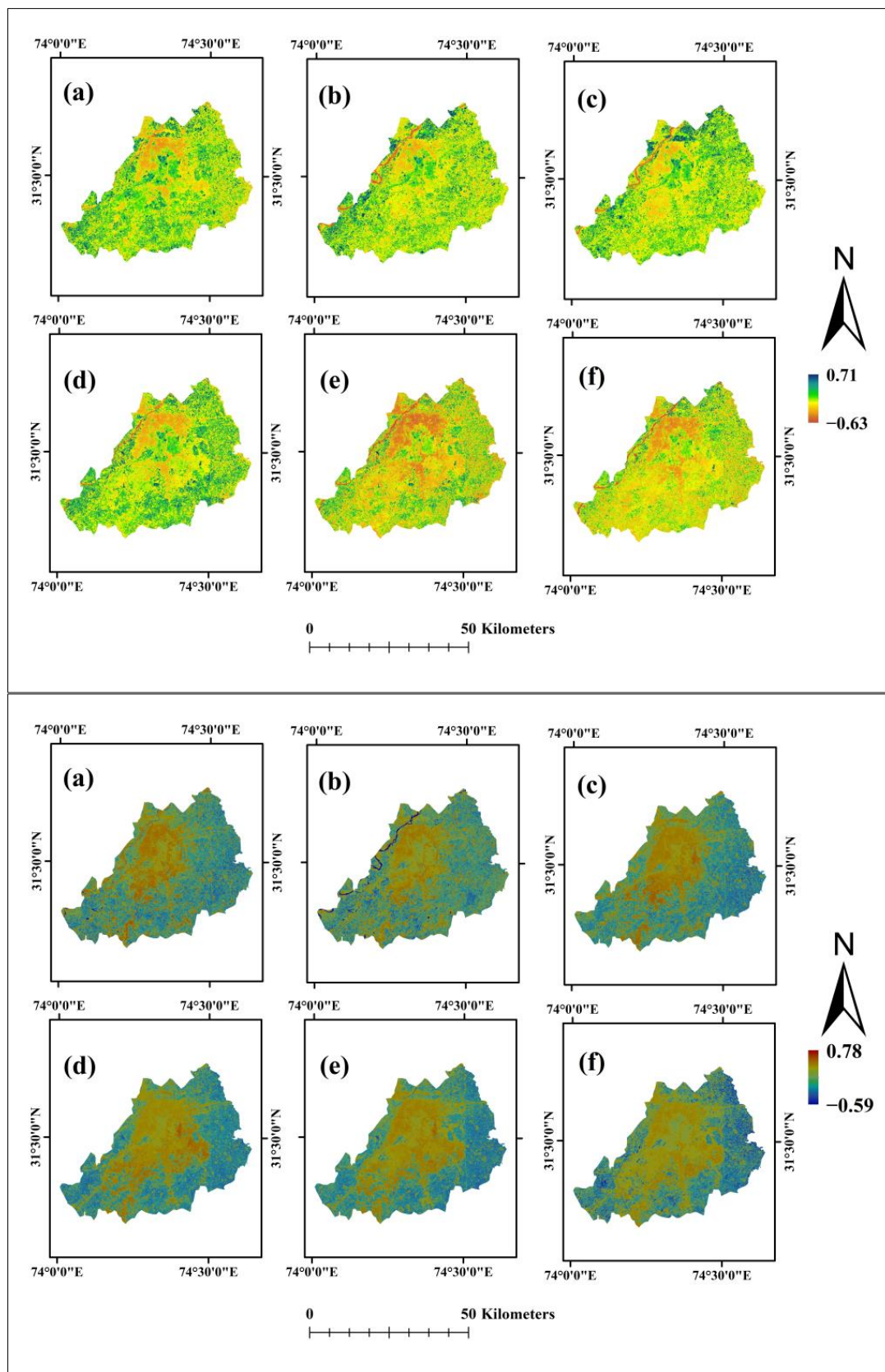
Figure 5. NDVI (Top) and NDBI (bottom) maps of Lahore city (ranging from −for the year (**a**) 1992, (**b**) 1996, (**c**) 2000, (**d**) 2008, (**e**) 2014, and (**f**) 2020.
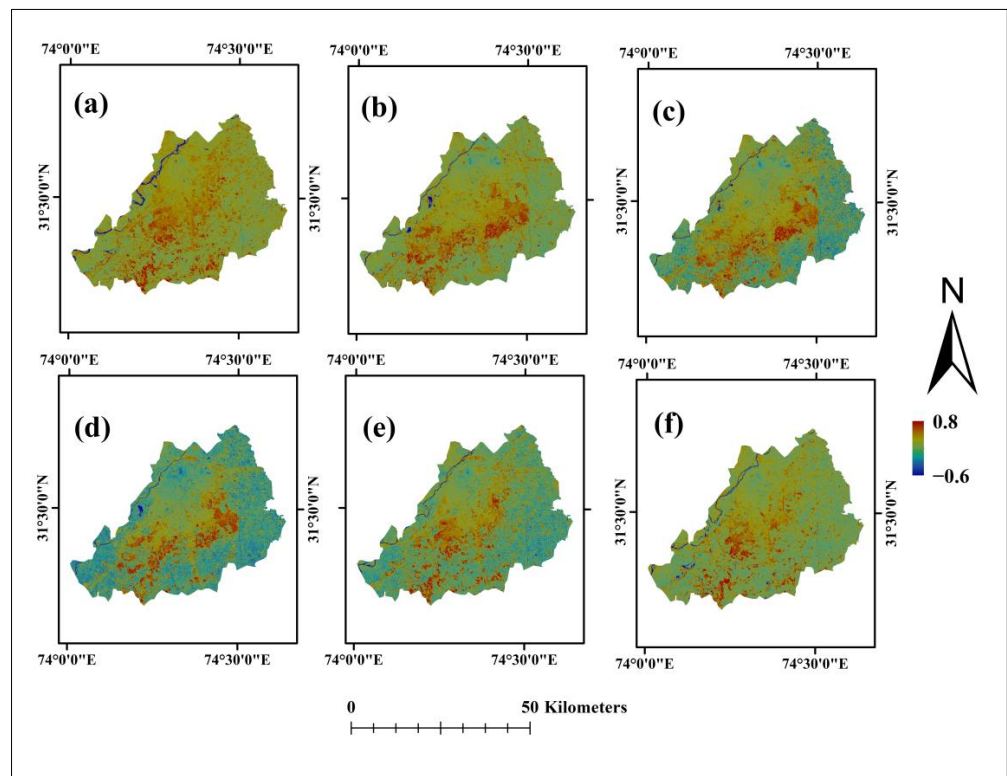
Figure 6. NDBaI map of Lahore for year (**a**) 1992, (**b**) 1996, (**c**) 2000, (**d**) 2008, (**e**) 2014, and (**f**) 2020.
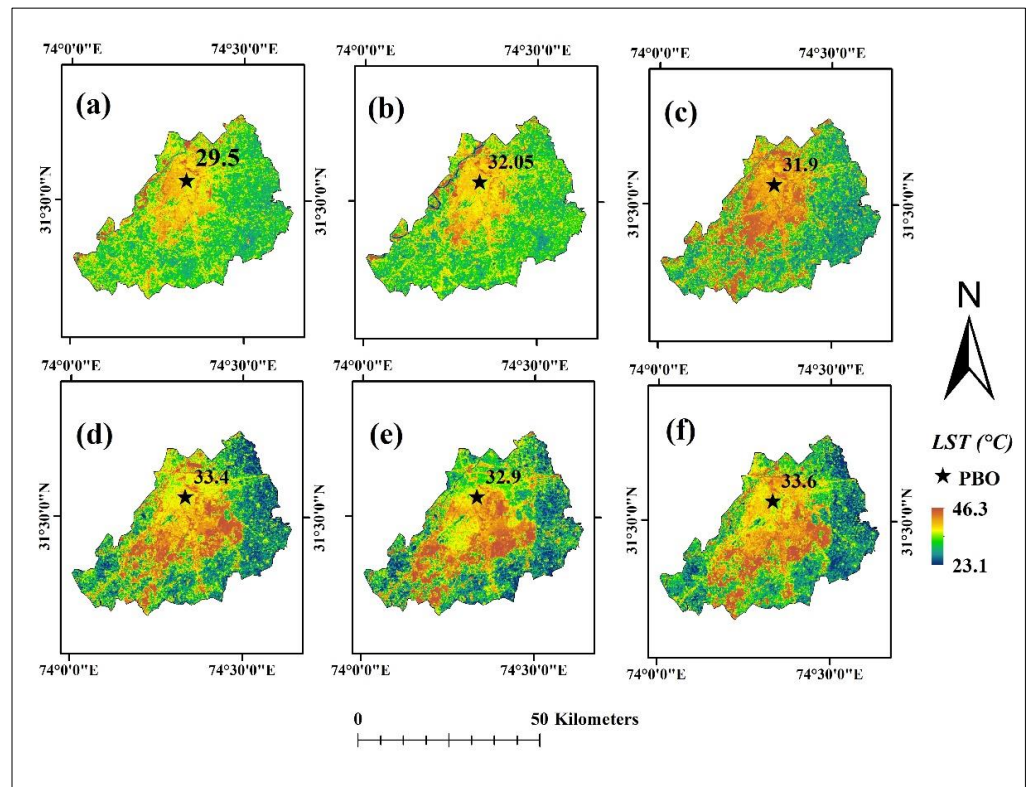
Figure 7. LST (°C) maps of Lahore for years (**a**) 1992, (**b**) 1996, (**c**) 2000, (**d**) 2008, (**e**) 2014, and (**f**) 2020. Star sign indicates the location of weather station.

Table 3. Spatiotemporal Distribution of LST.

LULC Types	Mean Estimated LST (°C) from Satellite Data *					
	1992	1996	2000	2008	2014	2020
Built-Up	28.4	30.5	33.5	31.45	34.3	35.35
Vegetation	25.9	29.1	28.5	26.2	29.3	30.7
Bare Land	34.5	35.7	33.1	32.6	36.8	37.2
Water	24.9	25.3	26.8	23.5	27.1	27.5

* An average LST value for all the pixels in particular LULC classes in specific Landsat based LST Image. Each value is the spatial mean of all the pixels belonging to the specific class in the image for specific year.

Moreover, temperature data (on image acquisition date), from the PMD weather station within the study area, was used for comparison and validation of the LST retrieved from the images [33]. The comparison revealed a slight variation in temperature (difference) between the image derived LST and the weather station data (Table 4). Positive and negative differences indicate the situations when the image derived LST is higher or lower than the temperature obtained from the weather station data, respectively. The observed differences were within a range of ± 2 °C and support the accuracy of the image derived LST [4,12,34].

Table 4. Comparison of air temperature recorded at the weather station and the surface temperature derived from the image at the same location (data collected from Lahore Pilot Balloon Observatory).

Date	LST (Landsat) °C	Air Temperature (Weather Station) °C	Temp. Difference (Landsat-Weather Station) °C
9 June 1992	28.4	29.5	−1.1
4 June 1996	30.5	32.05	−1.55
30 May 2000	33.5	31.9	1.6
5 June 2008	31.45	33.4	−1.95
6 June 2014	34.3	32.9	1.4
7 June 2020	35.35	33.6	1.75

3.4. LST vs. Spectral Indices

The NDVI values can be used as an important measure for the density of vegetation and the evaluation of variation in temperature [7,35]. These are the mean values obtained for each index and LST in association with the LULC classes. The mean pixel value for each LULC (average of all the pixels in a particular LULC class for a specific year) against the respective Index and LST were used to compare LST and the respective index in association with the LULC classes. A regression analysis was performed between the NDVI values of different LULCs and LST which showed a strong negative relationship (Figure 8). Such a negative relationship has also been reported by many relevant studies [27,36]. For the years 2014 and 2020, higher mean LST and lower mean NDVI values of built-up area and bare land were observed. In 2008, due to high precipitation and moisture a linear negative trend was observed, with vegetation having the minimum LST and maximum NDVI, opposite to bare land and built-up area, which had high LST and low NDVI, respectively.
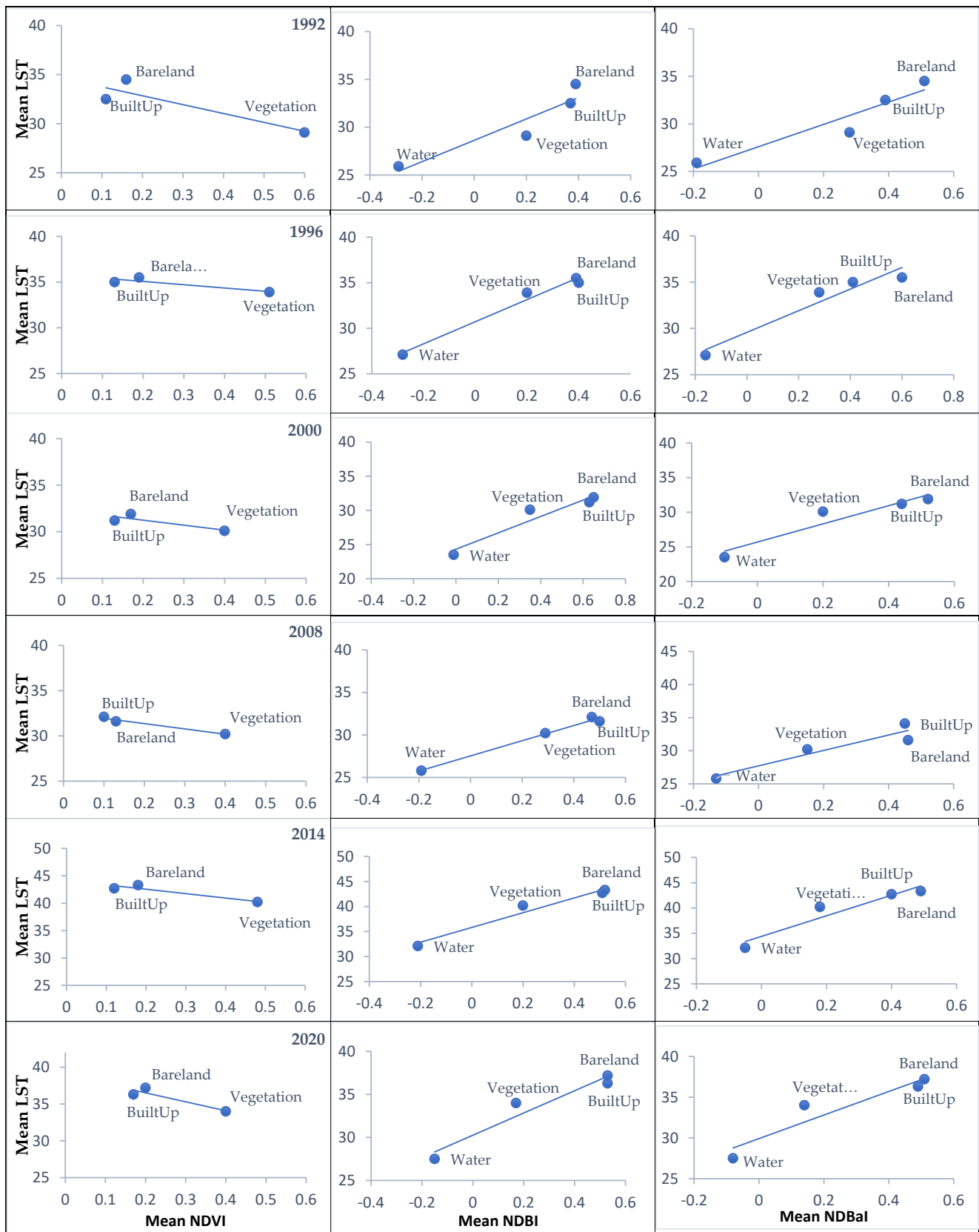
Figure 8. Scatterplots of mean NDVI, NDBI and NDBaI values vs. LST in association with LULC from 1992 to 2020. Each point is the mean value obtained for each index, and LST in association with LULC classes.

The relationship between LST and NDBI are also plotted and illustrated in Figure 9. Although the correlation was reasonable for the selected years, the spectral similarity of built-up area and bare land in the respective bands used in NDBI made it difficult to distinguish these two classes, whereas the NDBaI data amply reduced this spectral confusion. The mean values of NDBaI for the corresponding LULC types confirmed the relationship between bareness and the corresponding LST and indicated a correlation among the three variables (LST, NDBaI, LULC). However, due to the presence of moisture in 2008, the LST for bare land dropped considerably, while that of built-up areas increased, thus making the temperature difference between them higher in accordance with their corresponding NDBaI values.
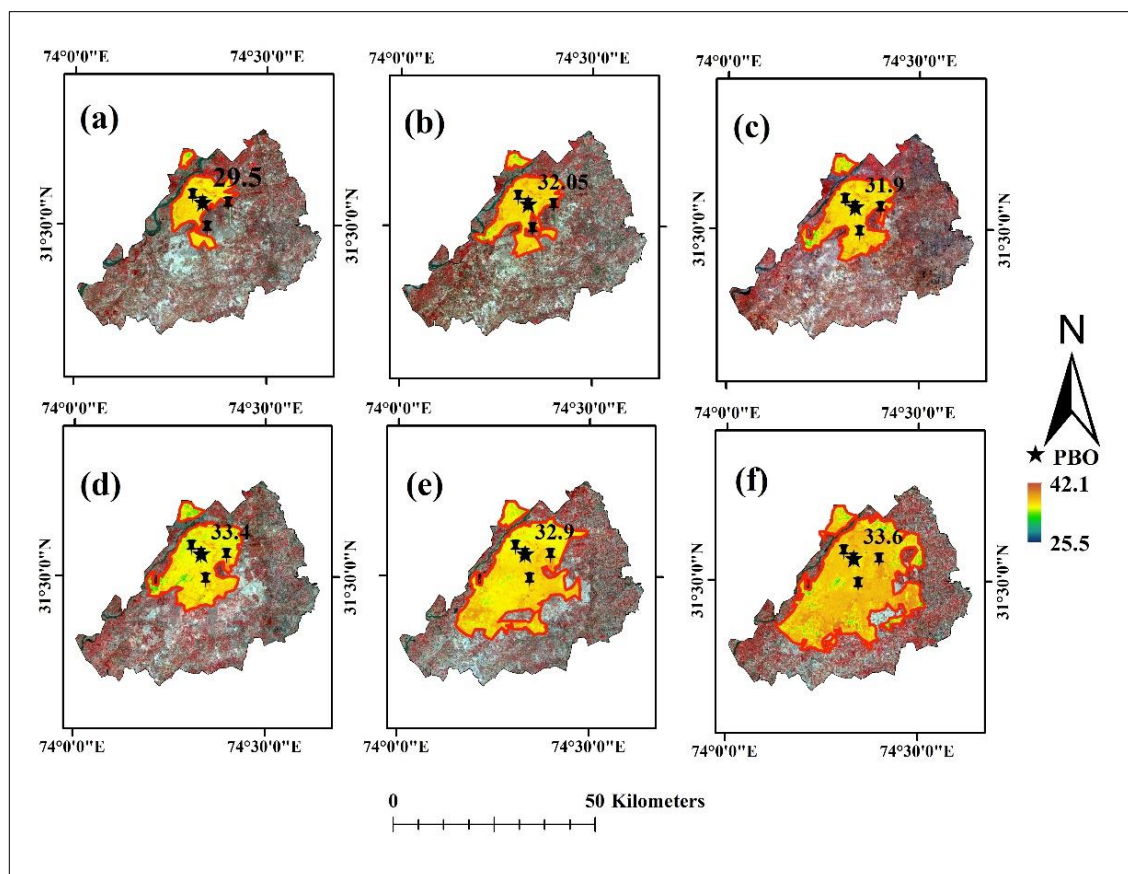
Figure 9. Expansion in Built-up land and LST in (**a**) 1992, (**b**) 1996, (**c**) 2000, (**d**) 2008, (**e**) 2014, (**f**) 2020. The symbol (★) indicates the position of Pilot Balloon Observatory (PBO).

3.5. Relationship between LST and LULC Pattern

Comparison of the temporal changes in LST and urban area extent from 1992 to 2020 showed an increasing trend in both variables. There was expansion in urban areas with time and consequently higher LST values were observed from satellite data in the same years. The increases in LST were also compared from ground weather stations (Pilot Balloon Observatory (PBO) to confirm the air temperature (Figure 9). A positive correlation between LST and built-up area (R = 0.65) was also observed (Figure 10), because, in our case, built-up area is a major driving factor due to the decrease in vegetation and bare land. This indicates that clearing of vegetative lands for buildings not only reduces the 'cooling effect' but those built-up areas also act as permanent source for urban microclimates.
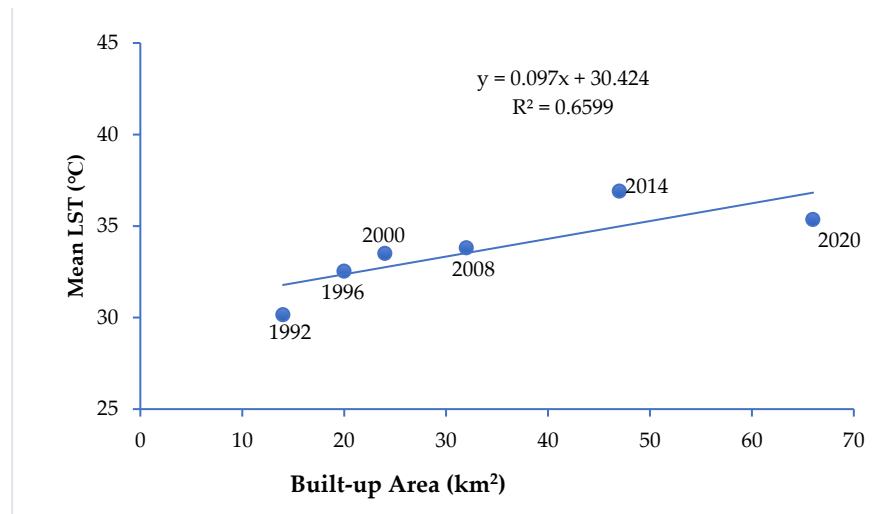
Figure 10. Relationship between Built-up area and LST.

3.6. Validation of LULC and LST and Future Trends

Future projections of LST and LULC were made by using the existing trend retrieved from the temporal satellite images (Figure 11a). To validate the future projection results, first, the trend for the year 2020 was predicted and then compared with the values retrieved from satellite images. The high correlation ($R^2 = 0.98$) suggests the reliability of the results for effective decision making (Figure 11b).
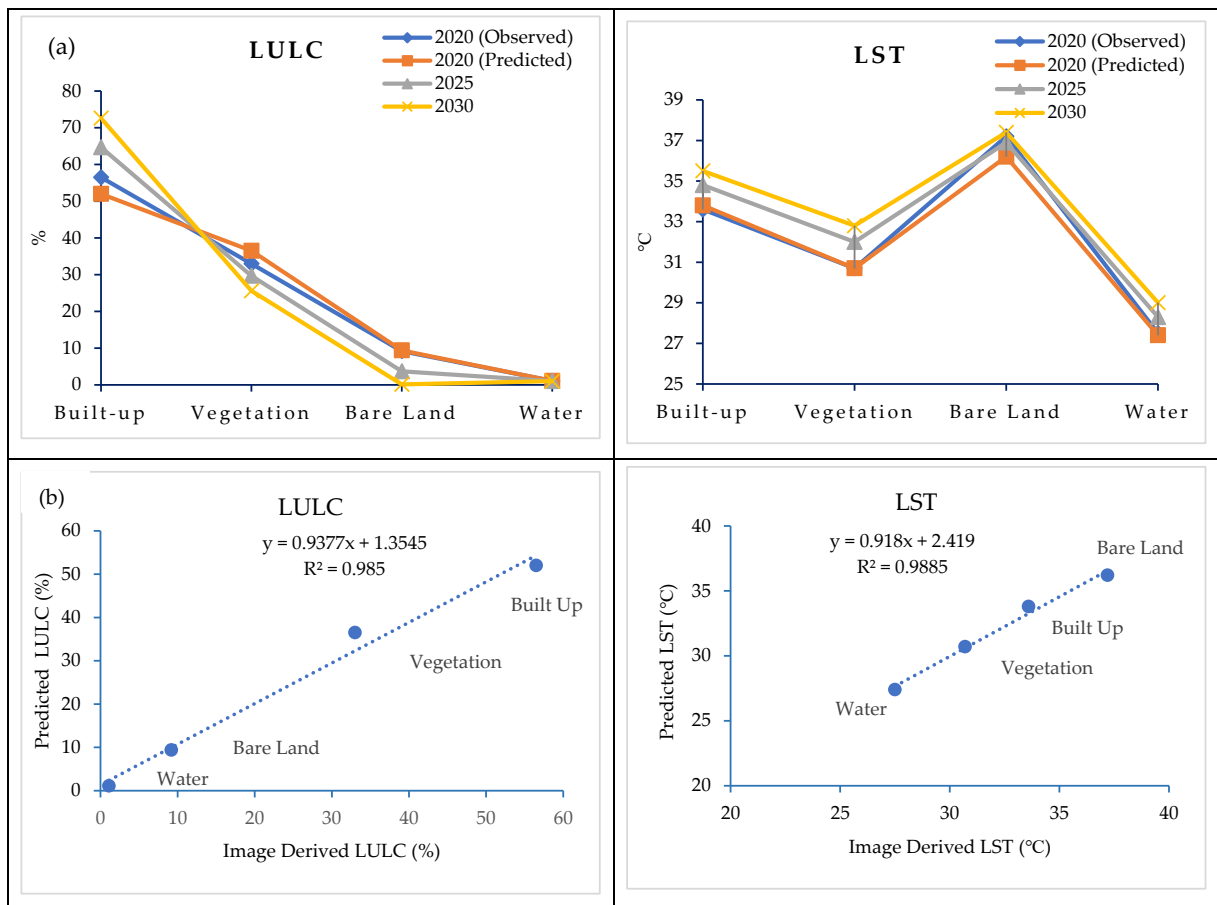
Figure 11. (**a**). LULC and LST's validation (for year 2020) and future prediction (for year 2025 and 2030), (**b**) Comparison of predicted and image derived LULC and LST for 2020.

It is worth mentioning that the difference in actual and predicted values for LULC remained within the range of 5% for built-up area, 3% for vegetation, and 1% for other LULCs (Table 5), whereas the LST differences remained within the range of 1 °C (Table 6). Moreover, the temperature predictions for LST suggest that mean temperature is continuously increasing and will be maximum for built-up and bare land rising to 37.4 °C in 2030 (Table 6). Although it looks like the temperature for bare land is highest, because bare land area is continuously decreasing, it will make less contribution to increasing temperature compared to the rapidly increasing built-up land. The LULC transformations show that the percent LULC area will be 1.01, 25.6, 72.5, and 0.14, for water, vegetation, built-up area, and bare land, respectively.

Table 5. Validation of percent change in LULC (by comparing predicted results for 2020 with the image derived results for the same year) and prediction for the year 2025 and 2030.

Years	Built-Up (%)	Vegetation (%)	Bare Land (%)	Water (%)
2020 (Image derived)	56.5	33	9.2	1.1
2020 (Predicted)	52	36.5	9.4	1.1
2025	64.7	29.7	3.7	1.05
2030	72.6	25.6	0.14	1.01

Table 6. Validation of change in LST (by comparing predicted results for 2020 with the image derived results for the same year) and prediction for the year 2021, 2025 and 2030.

Year	Built-Up (°C)	Vegetation (°C)	Bare Land (°C)	Water (°C)
2020 (Image Derived)	33.6	30.7	37.2	27.5
2020 (Predicted)	33	30.7	36.2	27.4
2025	34.8	32	36.9	28.3
2030	35.5	32.8	37.4	29.01

4. Discussion

This study focused on examining the relationship between LST and LULC changes in Lahore, using temporal remote sensing data from 1992 to 2020. The NDVI, NDBI and NDBaI indices as LULC indicators were found to be associated with LST and can efficiently be used to assess the urban climate and ecosystems. The results showed that LST is more influenced by LULC changes such as built-up area and bare land surface, while green areas (vegetation) and water bodies have lower impact on LST [37]. This has a multifaceted impact in urban areas like Lahore, where expansion of built-up area is at the expense of vegetative areas, not the barren lands, as the trend of increase in built-up area is in the SW and NE sides of the city by invading agricultural lands. Thus, increasing vegetation for a cooling effect has a positive effect on the ecosystem and can help to improve climate change. However, this is still not enough to balance the temperature rise caused by increased built-up area. Therefore, it is important for urban planners and administrators to think of some out-of-the-box solutions for redesigning and modification of buildings along with focusing on revegetation to achieve effective mitigation of urban climates while increasing green spaces [13]. This also indicates that bare lands are already decreasing, which means that in future, the major controlling factor of LST will be build-up area, thus strict policies on luxurious lateral expansions and illegal developments might be more effective solutions [20].

A suitable validation is essential for any satellite retrieved LST result by in situ measured data [38,39]. Comparison of the LST with a set of air temperature data recorded by ground stations at the time of satellite passes (approx.) was performed, as done previously in some studies [40–42]. This approach was followed considering the reported direct relationship between surface temperature and air temperature [38,43]. Quantitative models describing the land cover and LST relationships were constructed using multivariate linear

regression analysis considering each pixel value. These, combined with analysis of LST and LULC maps, indicated an evident increase in LST in 25 years depicting significant coherence between the urban thermal patterns and spatial distribution of urban LULCs [44–46]. Similar findings have also been found in other cities such as Rajshahi [47] and Dhaka [48] in Bangladesh and Ibadan-Nigeria [7]. Results indicate that there was an increase of about 41% in built-up area, whereas vegetation cover, bare land, and water declined by 24%, 17%, and 0.4%, respectively, confirming that built-up areas raise LST and, correspondingly, air temperature, whereas vegetation and water add lower LST; similar findings were also reported earlier [32,35]. Moreover, the overall classification accuracy for all the images was found good (in the range of 90 to 95%). However, there it was also observed that spatial distribution of different LULCs in the city tend to affect the variations in LST, which in turn, determine spatial thermal patterns and intensities. Quantitative analysis between LST and the indices revealed differences in temperature within an LULC, apart from those amongst various LULC types. A strong positive correlation between NDBI, NDBaI, and LST, illustrated the significant contribution of built-up area and bare land towards the rise in urban temperature [27]. By comparing the urban temperature with other land uses, it was found that after bare land, built-up area has the highest temperature. However, as the bare land has been reduced, built-up area has the higher contribution in land surface and thus towards air temperature rise.

5. Conclusions

Assessing the LST and its relationship with LULC using spectral indices from remote sensing help to track local climate and air temperature efficiently, however, use of multiple algorithms or models, along with adding higher number of observations or ground truthing, will add confidence for future predictions. The observed increase in the surface and near surface temperature is leads to increasing LST and is attributed to the LULC changes (percentage of perviousness to imperviousness) and mainly the depletion of natural vegetation cover. The affects can also be attributed to poor land use planning and implementation, and inconsistent government policies. However, there is dire need of detailed mapping of this phenomenon using fine spatial resolutions to refine information and suggest to policy makers and city manager to seek site-specific potentials, risk and solutions. These results can help in policy- and decision-making for the improvement of ecological environments in future development plans for Lahore and other cities, to make them 'liveable' and thereby reduce their environmental footprints and limit other urban disasters.

using ArcGIS 10.4 and QGIS platforms and we are also thankful to Esri® and Open-Source Geospatial Foundation (OSGeo) and their development teams for this.

References

1. Nguyen, T.M.; Lin, T.-H.; Chan, H.-P. The Environmental Effects of Urban Development in Hanoi, Vietnam from Satellite and Meteorological Observations from 1999–2016. *Sustainability* **2019**, *11*, 1768. [CrossRef]
2. Ziter, C.D.; Pedersen, E.J.; Kucharik, C.J.; Turner, M.G. Scale-Dependent Interactions between Tree Canopy Cover and Impervious Surfaces Reduce Daytime Urban Heat during Summer. *Proc. Natl. Acad. Sci. USA* **2019**, *116*, 7575–7580. [CrossRef] [PubMed]
3. Alexander, C. Influence of the Proportion, Height and Proximity of Vegetation and Buildings on Urban Land Surface Temperature. *Int. J. Appl. Earth Obs. Geoinf.* **2021**, *95*, 102265. [CrossRef]
4. Srivastava, P.K.; Majumdar, T.J.; Bhattacharya, A.K. Surface Temperature Estimation in Singhbhum Shear Zone of India Using Landsat-7 ETM+ Thermal Infrared Data. *Adv. Sp. Res.* **2009**, *43*, 1563–1574. [CrossRef]
5. Zhang, H.; Zhao, X.; Kang, M.Y.; Han, J.J. Contrasting Changes in Fine-Scale Land Use Structure and Summertime Thermal Environment in Downtown Shanghai. *Sustain. Cities Soc.* **2022**, *83*, 103965. [CrossRef]
6. Yang, J.; Zhan, Y.; Xiao, X.; Xia, J.C.; Sun, W.; Li, X. Investigating the Diversity of Land Surface Temperature Characteristics in Different Scale Cities Based on Local Climate Zones. *Urban Clim.* **2020**, *34*, 100700. [CrossRef]
7. Ayanlade, A.; Aigbiremolen, M.I.; Oladosu, O.R. Variations in Urban Land Surface Temperature Intensity over Four Cities in Different Ecological Zones. *Sci. Rep.* **2021**, *11*, 20537. [CrossRef]
8. Al Kafy, A.; Al Faisal, A.; Rahman, M.S.; Islam, M.; Al Rakib, A.; Islam, M.A.; Khan, M.H.H.; Sikdar, M.S.; Sarker, M.H.S.; Mawa, J.; et al. Prediction of Seasonal Urban Thermal Field Variance Index Using Machine Learning Algorithms in Cumilla, Bangladesh. *Sustain. Cities Soc.* **2021**, *64*, 102542. [CrossRef]
9. Khan, S.; Gul, S.; Li, W. Remote Sensing Evaluation of Land Surface Temperature and Urban Area Expansion in Zhengzhou City during 2013–2015. *Nat. Appl. Sci. Int. J.* **2021**, *2*, 39–55. [CrossRef]
10. Saleem, M.S.; Ahmad, S.R.; Shafiq-Ur-Rehman; Javed, M.A. Impact Assessment of Urban Development Patterns on Land Surface Temperature by Using Remote Sensing Techniques: A Case Study of Lahore, Faisalabad and Multan District. *Environ. Sci. Pollut. Res.* **2020**, *27*, 39865–39878. [CrossRef]
11. Swamy, G.S.; Nagendra, S.M.; Schlink, U. Impact of Urban Heat Island on Meteorology and Air Quality at Microenvironments. *J. Air Waste Manag. Assoc.* **2020**, *70*, 876–891. [CrossRef] [PubMed]
12. Fu, P.; Weng, Q. A Time Series Analysis of Urbanization Induced Land Use and Land Cover Change and Its Impact on Land Surface Temperature with Landsat Imagery. *Remote Sens. Environ.* **2016**, *175*, 205–214. [CrossRef]
13. Abir, F.A.; Ahmmed, S.; Sarker, S.H.; Fahim, A.U. Thermal and Ecological Assessment Based on Land Surface Temperature and Quantifying Multivariate Controlling Factors in Bogura, Bangladesh. *Heliyon* **2021**, *7*, e08012. [CrossRef] [PubMed]
14. Zhang, Y.; Sun, L. Spatial-Temporal Impacts of Urban Land Use Land Cover on Land Surface Temperature: Case Studies of Two Canadian Urban Areas. *Int. J. Appl. Earth Obs. Geoinf.* **2019**, *75*, 171–181. [CrossRef]
15. Aksu, O.; Iban, M.C. Considerations on the Land Management System Approach in Turkey by the Experiences of a Case Study. *Surv. Rev.* **2019**, *51*, 87–96. [CrossRef]
16. Wemegah, C.S.; Yamba, E.I.; Aryee, J.N.A.; Sam, F.; Amekudzi, L.K. Assessment of Urban Heat Island Warming in the Greater Accra Region. *Sci. Afr.* **2020**, *8*, e00426. [CrossRef]
17. Kafy, A.-A.; Naim, N.H.; Khan, M.H.H.; Islam, M.A.; Al Rakib, A.; Al-Faisal, A.; Sarker, M.H.S. Prediction of Urban Expansion and Identifying Its Impacts on the Degradation of Agricultural Land. In *Re-envisioning Remote Sensing Applications*; CRC Press: Boca Raton, FL, USA, 2021; pp. 85–106. [CrossRef]
18. Meng, F.; Liu, M. Remote-Sensing Image-Based Analysis of the Patterns of Urban Heat Islands in Rapidly Urbanizing Jinan, China. *Int. J. Remote Sens.* **2013**, *34*, 8838–8853. [CrossRef]
19. Ahmad, A.; Gilani, H.; Shirazi, S.A.; Pourghasemi, H.R.; Shaukat, I. Spatiotemporal Urban Sprawl and Land Resource Assessment Using Google Earth Engine Platform in Lahore District, Pakistan. In *Computers in Earth and Environmental Sciences*; Elsevier: Amsterdam, The Netherlands, 2022; pp. 137–150.
20. Imran, M.; Aqsa, M. Analysis and Mapping of Present and Future Drivers of Local Urban Climate Using Remote Sensing: A Case of Lahore, Pakistan. *Arab. J. Geosci.* **2020**, *13*, 278. [CrossRef]
21. Khalil, U.; Aslam, B.; Azam, U.; Khalid, H.M.D. Time Series Analysis of Land Surface Temperature and Drivers of Urban Heat Island Effect Based on Remotely Sensed Data to Develop a Prediction Model. *Appl. Artif. Intell.* **2021**, *35*, 1803–1828. [CrossRef]
22. Zhang, X.; Zhong, T.; Wang, K.; Cheng, Z. Scaling of Impervious Surface Area and Vegetation as Indicators to Urban Land Surface Temperature Using Satellite Data. *Int. J. Remote Sens.* **2009**, *30*, 841–859. [CrossRef]
23. Haas, J.; Ban, Y. Urban Growth and Environmental Impacts in Jing-Jin-Ji, the Yangtze, River Delta and the Pearl River Delta. *Int. J. Appl. Earth Obs. Geoinf.* **2014**, *30*, 42–55. [CrossRef]

24. Yang, Y.Z.; Cai, W.H.; Yang, J. Evaluation of MODIS Land Surface Temperature Data to Estimate Near-Surface Air Temperature in Northeast China. *Remote Sens.* **2017**, *9*, 410. [CrossRef]
25. Akbar, T.A.; Hassan, Q.K.; Ishaq, S.; Batool, M.; Butt, H.J.; Jabbar, H. Investigative Spatial Distribution and Modelling of Existing and Future Urban Land Changes and Its Impact on Urbanization and Economy. *Remote Sens.* **2019**, *11*, 105. [CrossRef]
26. Kappa Coefficient Confusion Matrices. Available online: https://www.l3harrisgeospatial.com/docs/calculatingconfusionmatrices.html (accessed on 13 August 2021).
27. Guha, S.; Govil, H.; Dey, A.; Gill, N. Analytical Study of Land Surface Temperature with NDVI and NDBI Using Landsat 8 OLI and TIRS Data in Florence and Naples City, Italy. *Eur. J. Remote Sens.* **2018**, *51*, 667–678. [CrossRef]
28. Nazir, A.; Ullah, S.; Saqib, Z.A.; Abbas, A.; Ali, A.; Iqbal, M.S.; Hussain, K.; Shakir, M.; Shah, M.; Butt, M.U. Estimation and Forecasting of Rice Yield Using Phenology-Based Algorithm and Linear Regression Model on Sentinel-II Satellite Data. *Agriculture* **2021**, *11*, 1026. [CrossRef]
29. Yuan, F.; Bauer, M.E. Comparison of Impervious Surface Area and Normalized Difference Vegetation Index as Indicators of Surface Urban Heat Island Effects in Landsat Imagery. *Remote Sens. Environ.* **2007**, *106*, 375–386. [CrossRef]
30. Landsat Project Science Office. *Landsat 7 Science Data User's Handbok*; NASA's Goddard Space Flight Center: Greenbelt, MD USA, 2002; 186p.
31. Bastiaanssen, W.G.M.; Menenti, M.; Feddes, R.A.; Holtslag, A.A.M. A Remote Sensing Surface Energy Balance Algorithm for Land (SEBAL)-1. Formulation. *J. Hydrol.* **1998**, *212*, 198–212. [CrossRef]
32. Sultana, S.; Satyanarayana, A.N.V.; Rinner, C.; Hussain, M. Toronto's Urban Heat Island—Exploring the Relationship between Land Use and Surface Temperature. *Remote Sens.* **2011**, *3*, 1251–1265. [CrossRef]
33. Xiong, Y.; Chen, F. Correlation Analysis between Temperatures from Landsat Thermal Infrared Retrievals and Synchronous Weather Observations in Shenzhen, China. *Remote Sens. Appl. Soc. Environ.* **2017**, *7*, 40–48. [CrossRef]
34. Qin, Q.; Zhang, N.; Nan, P.; Chai, L. Geothermal Area Detection Using Landsat ETM+ Thermal Infrared Data and Its Mechanistic Analysis—A Case Study in Tengchong, China. *Int. J. Appl. Earth Obs. Geoinf.* **2011**, *13*, 552–559. [CrossRef]
35. Kabano, P.; Lindley, S.; Harris, A. Evidence of Urban Heat Island Impacts on the Vegetation Growing Season Length in a Tropical City. *Landsc. Urban Plan.* **2021**, *206*, 103989. [CrossRef]
36. Mudede, M.F.; Newete, S.W.; Abutaleb, K.; Nkongolo, N. Monitoring the Urban Environment Quality in the City of Johannesburg Using Remote Sensing Data. *J. Afr. Earth Sci.* **2020**, *171*, 103969. [CrossRef]
37. Guha, S.; Govil, H.; Mukherjee, S. Dynamic Analysis and Ecological Evaluation of Urban Heat Islands in Raipur City, India. *J. Appl. Remote Sens.* **2017**, *11*, 036020. [CrossRef]
38. Vancutsem, C.; Ceccato, P.; Dinku, T.; Connor, S.J. Evaluation of MODIS Land Surface Temperature Data to Estimate Air Temperature in Different Ecosystems over Africa. *Remote Sens. Environ.* **2010**, *114*, 449–465. [CrossRef]
39. Naim, M.N.H.; Kafy, A.A. Assessment of Urban Thermal Field Variance Index and Defining the Relationship between Land Cover and Surface Temperature in Chattogram City: A Remote Sensing and Statistical Approach. *Environ. Chall.* **2021**, *4*, 100107. [CrossRef]
40. Goldblatt, R.; Addas, A.; Crull, D.; Maghrabi, A.; Levin, G.G.; Rubinyi, S. Remotely Sensed Derived Land Surface Temperature (LST) as a Proxy for Air Temperature and Thermal Comfort at a Small Geographical Scale. *Land* **2021**, *10*, 410. [CrossRef]
41. Addas, A.; Goldblatt, R.; Rubinyi, S. Utilizing Remotely Sensed Observations to Estimate the Urban Heat Island Effect at a Local Scale: Case Study of a University Campus. *Land* **2020**, *9*, 191. [CrossRef]
42. Weng, Q.; Firozjaei, M.K.; Sedighi, A.; Kiavarz, M.; Alavipanah, S.K. Statistical Analysis of Surface Urban Heat Island Intensity Variations: A Case Study of Babol City, Iran. *GIScience Remote Sens.* **2019**, *56*, 576–604. [CrossRef]
43. Benali, A.; Carvalho, A.C.; Nunes, J.P.; Carvalhais, N.; Santos, A. Estimating Air Surface Temperature in Portugal Using MODIS LST Data. *Remote Sens. Environ.* **2012**, *124*, 108–121. [CrossRef]
44. Faqe Ibrahim, G.R. Urban Land Use Land Cover Changes and Their Effect on Land Surface Temperature: Case Study Using Dohuk City in the Kurdistan Region of Iraq. *Climate* **2017**, *5*, 13. [CrossRef]
45. Chen, X.L.; Zhao, H.M.; Li, P.X.; Yin, Z.Y. Remote Sensing Image-Based Analysis of the Relationship between Urban Heat Island and Land Use/Cover Changes. *Remote Sens. Environ.* **2006**, *104*, 133–146. [CrossRef]
46. Chen, A.; Yao, X.A.; Sun, R.; Chen, L. Effect of Urban Green Patterns on Surface Urban Cool Islands and Its Seasonal Variations. *Urban For. Urban Green.* **2014**, *13*, 646–654. [CrossRef]
47. Al Kafy, A.; Al-Faisal, A.; Mahmudul Hasan, M.; Sikdar, M.S.; Hasan Khan, M.H.; Rahman, M.; Islam, R. Impact of LULC Changes on LST in Rajshahi District of Bangladesh: A Remote Sensing Approach. *J. Geogr. Stud.* **2020**, *3*, 11–23. [CrossRef]
48. Ahmed, B.; Kamruzzaman, M.D.; Zhu, X.; Shahinoor Rahman, M.D.; Choi, K. Simulating Land Cover Changes and Their Impacts on Land Surface Temperature in Dhaka, Bangladesh. *Remote Sens.* **2013**, *5*, 5969–5998. [CrossRef]